Surface Behavior in Deuterium Permeation through Erbium Oxide Coating

T. Chikada 1), A. Suzuki 1), C. Adelhelm 2), T. Terai 1), T. Muroga 3)

1) The University of Tokyo, Tokyo, Japan
2) Max-Planck-Institut für Plasmaphysik, Garching, Germany
3) National Institute for Fusion Science, Toki, Japan

E-mail contact of main author: chikada@nuclear.jp

Abstract. Suppression of tritium permeation through structural materials is essential in order to mitigate the fuel loss and radioactive concerns. Ceramic coatings have been investigated for over three decades as tritium permeation barriers, however, a very limited number of investigations on hydrogen-isotope permeation mechanism through the coatings have been reported. In this study, deuterium permeation behaviors of erbium oxide coatings fabricated by filtered arc deposition on reduced activation ferritic/martensitic steels have been investigated. The samples coated on both sides of the substrates show remarkably lower permeability than those coated on one side, and the maximum reduction efficiency indicates a factor of 10^5 compared to the substrate. The different permeation behaviors between the dissociation/solution and the recombination/desorption sides of the coatings have been found by the crystal structure analysis and the evaluation of the energy barriers. It is finally concluded that the permeation processes on the front and back surfaces are independent, and the TPB efficiency of the samples coated on both sides can be expressed by a multiplication of that of each side.

1. Introduction

Toward the realization of DEMO reactors and commercial fusion power plants, establishing an efficient fuel cycle, especially tritium breeding and recovering, is indispensable. Since the 1970s, the consideration for tritium-material interactions has been pointed out and the necessity of suppression of tritium permeation through structural materials has come to public attention. Reduced activation ferritic/martensitic (RAFM) steels which are candidate structural materials for DEMO reactors actually have high permeability of hydrogen isotopes in the operational temperature range. In order to mitigate the tritium permeation to an acceptable level, the fabrication of thin ceramic coatings as tritium permeation barriers (TPBs) has been studied for three decades [1–5].

Erbium oxide (Er_2O_3) coatings have recently been investigated as a TPB as well as an electrical insulating coating for a self-cooled lithium blanket system [6,7]. It has been found that the Er_2O_3 coatings can suppress deuterium permeation to an extent similar to other candidate coating materials [8,9]. Furthermore, the precise microstructure analyses and the permeation measurements for the coatings have clarified the advantages as a TPB: the low deposition temperature [10], the thermal-cycle endurance [11], and the possibility for a plant-scale fabrication [12]. However, no interpretations for the whole permeation process and the expression mechanism of permeation reduction of the coatings have been given yet. Therefore, the goal of this work is to discuss the elementary steps in the deuterium permeation through the coating, especially on the surface of the coating.

2. Experimental Details

2.1. Sample Preparation

Two kinds of RAFM steels, F82H (8Cr-2W, Heat No. 9753 42W-4) and JLF-1 (9Cr-2W), were used as substrate materials. In this study, they were used in the same way because the

permeation properties of both materials are quite similar [10]. Disk-shaped substrates of 20 mm in diameter and 0.5 mm in thickness were mirror polished. Er_2O_3 coatings were fabricated by a filtered arc deposition device described in references [8,13]. A radio frequency (RF)-induced bias voltage of −150 V was applied to the substrate to accelerate the Er ions. Substrate temperature during deposition was at room temperature for avoiding the formation of the oxide layer on the substrate which caused peeling of the coating [11]. The coating was deposited on one side or both sides of the substrate and the thickness of the coating was 1.3 or 2.6 μm.

2.2. Characterization Technique

The scheme and the configuration for deuterium permeation measurements are described in detail in the previous study [10]. Two vacuum chambers divided by a sample are separately evacuated up to about 10^{-6} Pa. Then deuterium (purity of 99.995%) is introduced into one side (called the high-pressure volume, HPV) at 10^4–10^5 Pa with a leak valve. Measuring partial pressure of deuterium permeating through the sample to another side (called the low-pressure volume, LPV) is performed by quadrupole mass spectrometer (QMS). The LPV chamber is continuously pumped during the experiments and the QMS works within the range of 10^{-10}–10^{-5} mol/m^{2}s for D_2 in this method with secondary electron multiplier. The sample coated on one side is basically mounted with the coating facing the HPV in order to avoid surface oxidation on the uncoated side of the sample by contamination molecules. Therefore, when the coating is facing with the LPV, surface oxidation on the uncoated side facing the HPV is required consideration [10].

The procedure of the permeation measurements is as follows. The coated sample is heated up to 873 K with an electric furnace before setting a test temperature to release remaining gases for a better vacuum condition. After the test temperature has become stable, the deuterium gas is introduced by 8.00×10^4 Pa at the HPV. When the deuterium signal observed from the QMS becomes stable, the deuterium pressure is decreased in sequence: e.g. 4.00×10^4, 2.00×10^4, and 1.00×10^4 Pa by opening a valve connected to the evacuation system of the upstream.

For the discussion of permeation behavior, the crystal structure of the coating before and after the permeation measurements was analyzed by X-ray diffraction (XRD).

3. Theory

The hydrogen-isotope permeation through the material can be expressed in principle by a multiplication of two predominant processes: solution and diffusion [14]. When hydrogen is solved in the material as the atomic state, the hydrogen solubility S (mol m^{-3}) is given by Sieverts' law:

$$S = K_S p^{0.5}, \qquad (1)$$

where K_S is Sieverts' constant (mol m^{-3} Pa$^{-0.5}$) and p is the hydrogen pressure (Pa). K_S and the hydrogen diffusivity D (m^2 s^{-1}) are thermally activated processes expressed by the Arrhenius rate equation:

$$K_S = K_{S0} \exp\left(-\frac{E_S}{RT}\right); \qquad (2)$$

$$D = D_0 \exp\left(-\frac{E_D}{RT}\right), \qquad (3)$$

where E_S and E_D are the simplified activation energies of solution and diffusion (J mol^{-1}), R is the gas constant (8.314 J K^{-1} mol^{-1}), and T is the temperature (K). Finally, the hydrogen permeation flux per unit area at steady-state J (mol m^{-2} s^{-1}) through the material of d (m) in thickness is expressed with the product of the equation (1) and (3):

$$J = K_S D \frac{p^{0.5}}{d}, \qquad (4)$$

where $K_S D$ is named the permeability P (mol m^{-1} s^{-1} Pa$^{-0.5}$) as the intrinsic parameter of the permeation. P is also a thermally activated process expressed as:

$$P = P_0 \exp\left(-\frac{E_P}{RT}\right), \qquad (5)$$

where E_P is the activation energy of permeation (J mol^{-1}) calculated by the sum of E_S and E_D.

It is noted that the simplest case of the permeation, where the rate-limiting process is the diffusion of hydrogen atoms through the solid, can satisfy the equations described above. When the permeation rate is limited by the surface processes such as absorption and desorption, the exponent of the driving pressure p will increase to 1. The pressure exponent can be estimated by changing the driving pressure under the fixed temperature.

4. Results

For the evaluation of the deuterium permeation regime of the Er_2O_3 coatings, the deuterium pressure dependence of the permeation flux has been investigated. Figures 1 and 2 illustrate the driving pressure dependence of the permeation flux of the one-side-coated and the both-side-coated samples. A linear relationship is confirmed for both samples in the double logarithmic plots of the data. The pressure exponent of the one-side-coated sample shows 0.50–0.61, indicating the permeation rate is limited by the diffusion of deuterium atoms. The proportional relationship between the square root of the driving pressure and the permeation flux is obvious especially at 873–973 K because of the clearer permeation signals than those at the lower temperatures. In the measurements for the both-side-coated sample, while there was an uncertainty to detect clear signals at 773 K, the permeation exponents of 0.49–0.54 are indicated. Therefore, these results allow us to apply the permeation theory described in the previous chapter to the coated samples.

The deuterium permeability was calculated by the equation (4) with the permeation flux and the sample thickness. The Arrhenius plots of the permeability of the substrate and the coatings are shown in figure 3. The permeabilities of the both-side-coated samples show one or two orders of magnitude lower than those of the one-side-coated samples. The thickness of the coatings on one side is nearly inversely proportional to the permeability, which means a proportional relationship between the permeability and the permeation distance. However, the permeability of the 1.3/1.3 μm-coated sample on both sides is much lower than that of the 2.6 μm-coated sample on one side in spite of the same effective coating thickness. The difference was highly reproducible, which indicates the existence of another factor which influences the permeation behavior as well as the permeation distance. Besides, from the viewpoint of the TPB efficiency, the 2.6/2.6 μm-coated sample on both sides reduced the permeability to $1/10^5$ at 873 K and $1/10^4$ at 973 K in comparison with the RAFM substrate. These values are remarkable and only a few past studies achieved by using the TiC/TiN multiple coatings [15,16] are comparable.

5. Discussion

It is essential to clarify the difference of permeation behavior of the one-side-coated and the both-side-coated samples. That means a necessity for the discussion about the permeation behavior of the both-side-coated samples at the front and back surfaces separately. Figure 4 shows the Arrhenius plots of the one-side coated samples facing the HPV and the LPV. The coating facing the LPV shows about 6 times higher permeabilities than that facing the HPV. It is noted that the uncoated metal surface of the sample has been oxidized by the impurities in the HPV as for the coating facing the LPV. Despite the formation of the oxide layer at the uncoated surface, the permeability is higher than that of the coating facing the HPV. It is obvious that the permeation behavior is different between the front and back surfaces of the coating. There are two possible explanations for the difference. One is that the rate of microstructural change of the coating facing the HPV might be much faster than that facing the LPV because the deuterium and impurities in each chamber (10^5 vs. 10^{-6} Pa) possibly affected the grain growth as reported in the previous study [17]. If the rate of the grain growth at the LPV is much slower than that at the HPV, the difference of the permeability will be reasonable. The other possible reason is the difference of the permeation process. Deuterium molecules dissociate into atoms and solve in the coating at the front surface, while the deuterium atoms recombine and the molecules are desorbed from the coating at the back surface. If one of the four processes, dissociation, solution, recombination, and desorption, is dominant in the permeation, the permeability will be different between the front and back surfaces.

The crystal states of the coatings before and after the permeation measurements were analyzed by using XRD. Firstly, the results of the samples after the short-term permeation measurements at high temperature and the powder diffraction file (PDF) of the cubic Er_2O_3 [18] are presented in figure 5. The spectrum (a) indicates the monoclinic B-phase Er_2O_3 which is determined in the reference [13], while the crystal structure transformed to the cubic C-phase after the deuterium permeation at 923–973 K for approximately 12 h as shown in (b) and (c). In addition, the intensity of the (4 0 0) peak at 34º in (b) is the strongest despite the (2 2 2) peak at 29º is the highest peak in the PDF. The intensities are basically corresponding to the PDF in spectrum (c), however, the (4 0 0) peak is still higher. It is proved that the crystal transformation behavior of the coatings is different between the HPV and the LPV.

Secondly, the results of the samples after the long-term permeation measurements at high temperature are shown in figure 6. Sample (d) is the spectrum of the one-side-coated sample after the permeation facing the LPV. Sample (e) and (f) is the spectra of the both-side-coated sample after the permeation facing the HPV and the LPV, respectively. By far the strongest (4 0 0) peak at 34° is seen in every spectrum, and the (6 0 0) peak which is particularly weak in the PDF is also detected at 52°. On the other hand, the main peaks in the PDF such as (2 2 2) disappeared. The iron oxide peak at 32° is considered to be detected from the uncoated area. These results mean the strong orientation in [1 0 0] direction has occurred after the exposure to the deuterium flux. Although there are a few differences between the spectrum (d) and (e)/(f), such as the (4 4 0) peak at 49°, those seem to be because of the exact durations and temperatures for the permeation measurements: at 923 K for 22 h for (d), and at 923 K for 8 h + at 973 K for 12 h for (e) and (f). To conclude, the rate of the transformation of the coating facing the LPV is slower than that facing the HPV, however, the crystal structure of the coatings has become congruent as a result of the long-term deuterium permeation at more than

923 K. Therefore, the microstructure-change rate at the front and back sides of the coating does not cause the difference of the permeability.

In order to discuss the permeation process at the front and back surfaces, the activation energies of permeation were calculated by the equation (5) with the Arrhenius plots shown in figure 3 and 4. The permeabilities of the one-side and both-side-coated samples were fitted as follows:

1) 2.6 μm on one side facing the HPV: $P_1 = 7.6\times10^{-9}\exp\left(-\frac{79(\mathrm{kJ\,mol^{-1}})}{RT}\right)$; (6)

2) 2.6 μm on one side facing the LPV: $P_2 = 7.3\times10^{-10}\exp\left(-\frac{59(\mathrm{kJ\,mol^{-1}})}{RT}\right)$; (7)

3) 1.3/1.3 μm on both sides: $P_3 = 8.0\times10^{-8}\exp\left(-\frac{117(\mathrm{kJ\,mol^{-1}})}{RT}\right)$; (8)

4) 2.6/2.6 μm on both sides: $P_4 = 3.5\times10^{-7}\exp\left(-\frac{142(\mathrm{kJ\,mol^{-1}})}{RT}\right)$. (9)

The activation energies of the both-side-coated samples are clearly higher than those of the one-side-coated samples. That indicates the existence of another contribution which largely affects the permeation properties other than the permeation distance. Since the same permeation distance is confirmed for samples 1–3, it is found that the higher activation energies have been brought not by the contribution of the diffusion process. In addition, the one-side-coated sample facing the LPV has the lower activation energy than that facing the HPV despite the formation of the oxide layer on the uncoated surface. It is suggested that the energy barrier of dissociation and solution of deuterium in the front surface is higher than those of recombination and desorption at the back surface. Furthermore, the activation energy of the both-side-coated sample is comparable to the sum of those of sample 1 and 2. This result raises an important finding that the permeation process on the front and back sides is independent, and the TPB efficiency of the both-side-coated sample is described not by an addition but by a multiplication of the TPB efficiency at the front and back surfaces. The TPB efficiency of the both-side-coated sample agrees well with the multiplication of those of the one-side-coated samples facing the HPV and the LPV shown in figure 4 considering an additional barrier by the oxidation of the uncoated side. The discussion held in this study can finally offer a proposal that TPBs should be designed with strong consideration for the surface contributions in order to obtain high permeation reduction efficiency: e.g. a multi-layered structure or a multi-pipe construction.

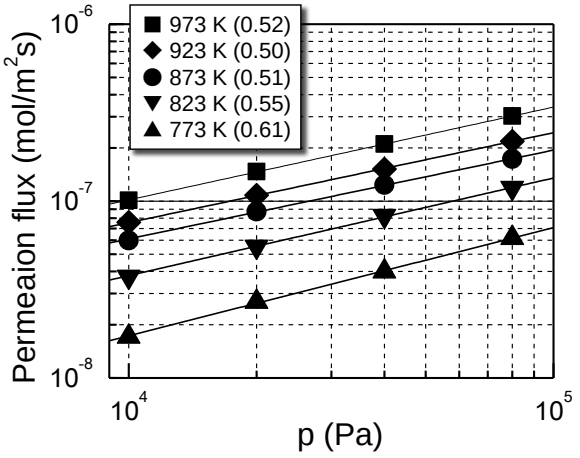

FIG. 1. Driving pressure dependence of deuterium permeation through the 1.3 μm-thick coating on one side of the JLF-1 substrate. Numbers in parenthesis represent the pressure exponents.

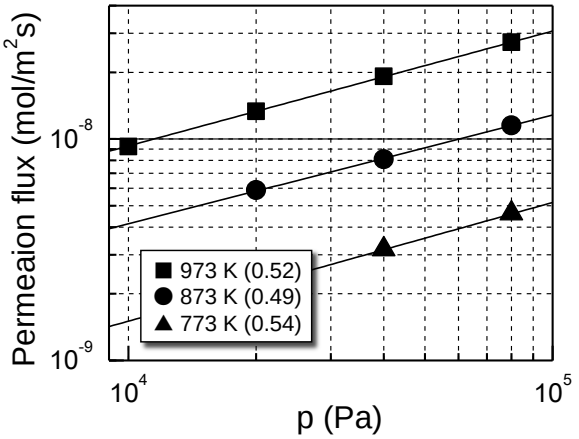

FIG. 2. Driving pressure dependence of deuterium permeation through the 1.3/1.3 μm-thick coatings on both sides of the JLF-1 substrate. Numbers in parenthesis represent the pressure exponents.

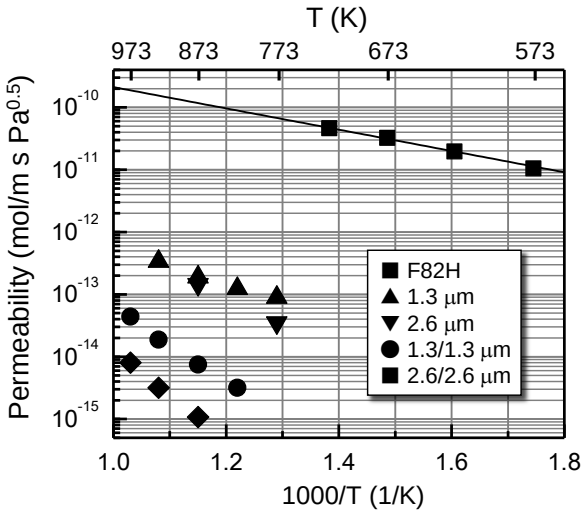

FIG. 3. Arrhenius plots of deuterium permeability of the substrate and the coated samples deposited on one side and both sides.

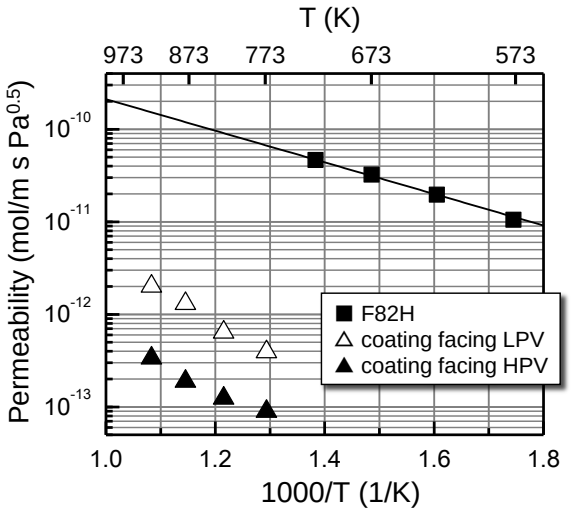

FIG. 4. Comparison of deuterium permeability between the 1.3 μm-thick coatings facing the HPV and the LPV.

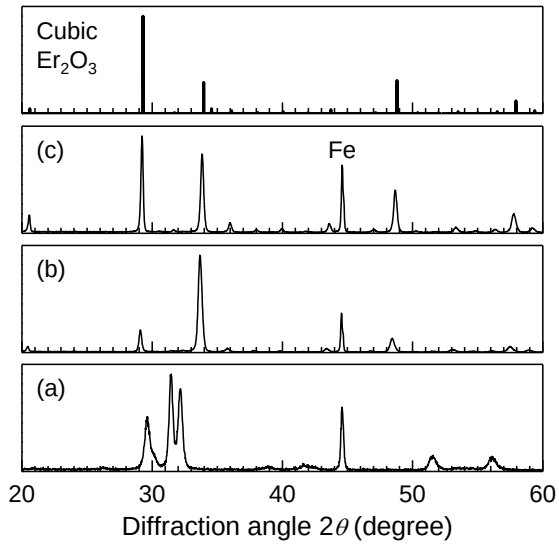

FIG. 5. XRD spectra of the coatings before and after the permeation measurements at 923–973 K for approximately 12 h: (a) as deposited, (b) the both-side-coated sample after the permeation measurements facing the HPV, and (c) facing the LPV. The powder diffraction file of the cubic C-phase Er_2O_3 is also given [21].

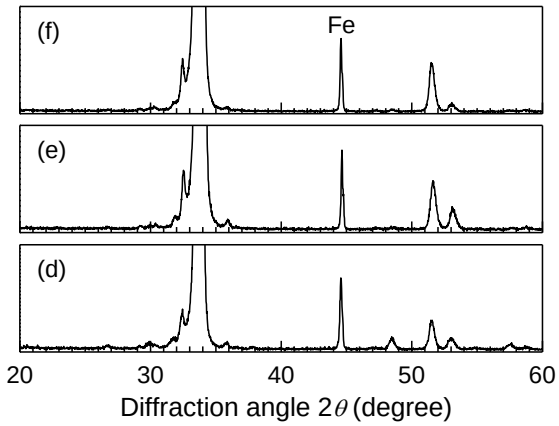

FIG. 6. XRD spectra of the coatings after the permeation measurements at 923–973 K for more than 20 h: (d) the one-side-coated sample facing the LPV, (e) the both-side-coated sample facing the HPV, and (f) facing the LPV.

6. Conclusion

Deuterium permeation properties of the Er_2O_3 coatings fabricated on one side and both sides of the RAFM steels by filtered arc deposition have been investigated. The coated samples show the rate limiting process by the diffusion of deuterium atoms. The both-side-coated samples indicate over one order of magnitude higher TPB efficiency than those of the one-side-coated samples with the same total coating thickness. The 2.6 μm-thick coating on both sides has reduced the permeability to $1/10^5$ in comparison with the bare RAFM steel at 873 K. The rate of the crystal transformation of the coatings facing the HPV is faster than that facing the LPV, however, the crystal structure has become similar after the long-term exposure to the deuterium flux at more than 923 K. The contribution of the surface phenomena has been clarified through the calculation of the activation energies of permeation. A string of considerations has lead to the finding that the permeation processes on the front and back

surfaces are independent, and the TPB efficiency can be expressed by a multiplication of that of each side.

Acknowledgements

This work was supported in part by KAKENHI (19055001), the Ministry of Education, Culture, Sports, Science and Technology, Japan, and Research Fellowships of the Japan Society for the Promotion of Science for Young Scientists.

References

[1] HOLLENBERG, G.W., et al., "Tritium/Hydrogen Barrier Development", Fusion Eng. Des. **28** (1995) 190.
[2] PERUJO, A., et al., "Tritium Permeation Barriers for Fusion Technology", Fusion Eng. Des. **28** (1995) 252.
[3] BENAMATI, G., et al., "Development of tritium permeation barriers on Al base in Europe", J. Nucl. Mater. **271&272** (1999) 391.
[4] KONYS, J., et al., "Status of Tritium Permeation Barrier Development in the EU", Fusion Sci. Technol. **47** (2005) 844.
[5] LEVCHUK, D., et al., "Deuterium Permeation through Eurofer and α-alumina Coated Eurofer", J. Nucl. Mater. **328** (2004) 103.
[6] PINT, B.A., et al., "Recent progress in the development of electrically insulating coatings for a liquid lithium blanket", J. Nucl. Mater. **329–333** (2004) 119.
[7] SAWADA, A., et al., "Fabrication of yttrium oxide and erbium oxide coatings by PVD methods", Fusion Eng. Des. **75–79** (2005) 737.
[8] KOCH, F., et al., "Crystallization Behavior of Arc-deposited Ceramic Barrier Coatings", J. Nucl. Mater. **329–333** (2004) 1403.
[9] LEVCHUK, D., et al., "Erbium oxide as a new promising tritium permeation barrier", J. Nucl. Mater. **367–370** (2007) 1033.
[10] CHIKADA, T., et al., "Deuterium permeation behavior of erbium oxide coating on austenitic, ferritic, and ferritic/martensitic steels", Fusion Eng. Des. **56** (2009) 309.
[11] CHIKADA, T., et al., "THERMAL INFLUENCE ON ERBIUM OXIDE COATING FOR TRITIUM PERMEATION BARRIER", Fusion Sci. Technol. **56** (2009) 309.
[12] CHIKADA, T., et al., "Microstructure control and deuterium permeability of erbium oxide coating on ferritic/martensitic steels by metal-organic decomposition", Fusion Eng. Des. in press (2010) doi:10.1016/j.fusengdes.2010.04.033.
[13] ADELHELM, C., et al., "Monoclinic B-phase erbium sesquioxide (Er_2O_3) thin films by filtered cathodic arc deposition", Scrip. Mater. **61** (2009) 789–792.
[14] STICKNEY, R.E., Diffusion and permeation of hydrogen isotopes in fusion reactors: A survey, The Chemistry of Fusion Technology, D.M. Gruen (Ed.), Plenum Press, New York, (1972) 241.
[15] SHAN, C., et al., "The behaviour of diffusion and permeation of tritium through 316L stainless steel with coating of TiC and TiN + TiC", J. Nucl. Mater. **191–194** (1993) 221.
[16] YAO, Z., et al., "The permeation of tritium through 316L stainless steel with multiple coatings", J. Nucl. Mater. **283–287** (2000) 1287.
[17] CHIKADA, T., et al., "Microstructure change and deuterium permeation behavior of erbium oxide coating", J. Nucl. Mater. in press.
[18] The Powder Diffraction File No. 77-0462, The International Centre for Diffraction Data.